Oil & Natural Gas Technology

DOE Award No.: DE-FE0009897

Quarterly Research Performance Progress Report (Period ending 03/31/2014)

Hydrate-Bearing Clayey Sediments: Morphology, Physical Properties, Production and Engineering/Geological Implications

Project Period (10/1/2012 to 9/30/2016)

Submitted by:
J. Carlos Santamarina

Georgia Institute of Technology
DUNS #: 097394084
505 10th street
Atlanta , GA 30332
e-mail: jcs@gatech.edu
Phone number: (404) 894-7605

Prepared for:
United States Department of Energy
National Energy Technology Laboratory

Submission date: 04/30/2014

Office of Fossil Energy

DISCLAIMER:

ACCOMPLISHMENTS

Context – Goals. *Fine grained sediments host more than 90% of the global gas hydrate accumulations. Yet, hydrate formation in clayey sediments is least understood and characterized. This research focuses on hydrate bearing clayey sediments. The goals of this research are (1) to gain a fundamental understanding of hydrate formation and ensuing morphology, (2) to develop laboratory techniques to emulate "natural" formations, (3) to assess and develop analytical tools to predict physical properties, (4) to evaluate engineering and geological implications, and (5) to advance gas production alternatives to recover methane from these sediments.*

Accomplished

The main accomplishments for this period include:

- CO_2 hydrate formation and X-ray imaging
- Thermal analysis of aluminum chamber
- Analysis of effective small-strain stiffness

Plan - Next reporting period

Design and fabricate two new chambers to conduct three hydrate formation experiments simultaneously. Fabricate rigid base for aluminum chamber for precise 3-D imaging. Experiment with different methods of forming gas hydrate in fine-grained sediments. Advance numerical solutions of large-strain stiffness and strength of various hydrate lens morphologies. Conduct measurements of physical properties of hydrate-bearing fine-grained sediments.

Research in Progress

CO_2 Hydrate Formation in Diatoms

CO_2 hydrate was formed in diatomaceous sediment within the X-ray transparent high-pressure sediment chamber.

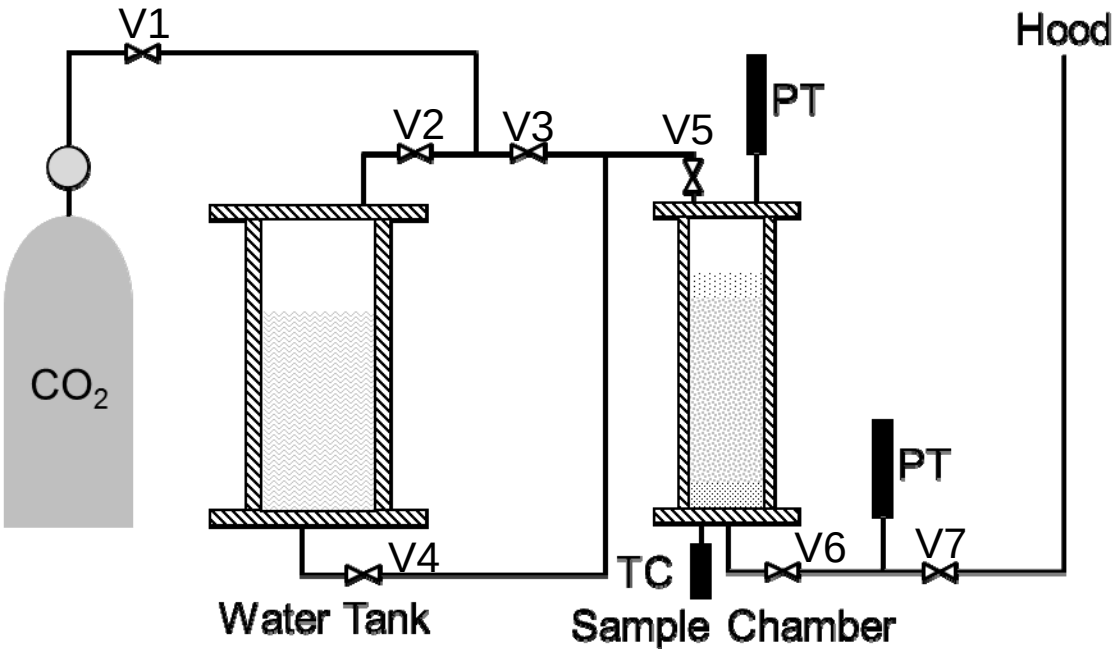

Figure 1. Schematic for the CO_2 hydrate formation experiment

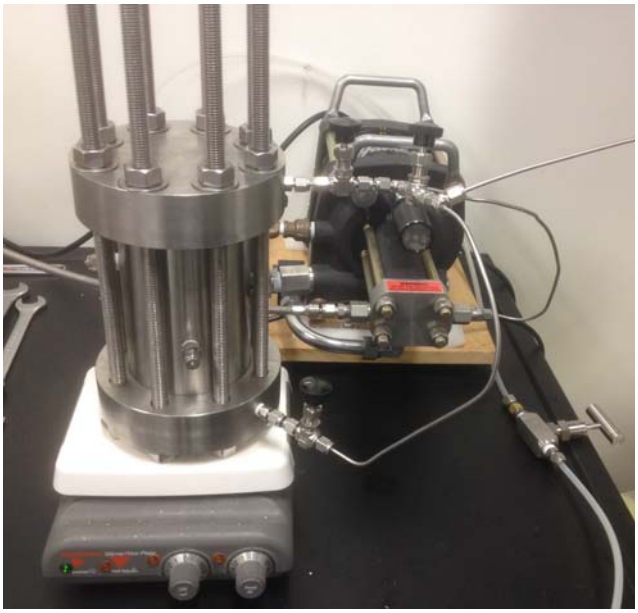

Figure 2. Gas booster and high pressure water tank (on top of stirrer)

Figure 3. Chamber and related pressure and temperature sensors (X-ray transparent high-pressure sediment chamber inside of the environmental chamber)

Sample preparation

Material order in the chamber from bottom to top:

1) filter paper (damp for good contact with the chamber cap)
2) silica flour (air dry)
3) diatom (oven dry)
4) coarse sand (air dry)

Two thermocouples were buried in the sample, one in the center and the other touching the wall (see X-ray projections).

Experimental procedure

1) Connect the system (schematic in figure 1).
2) Perform multiple vacuum-pressurization (2MPa) cycles of the diatom-filled chamber at room temperature (about 22°C) to minimize the presence of nitrogen and to fill all pores with CO_2.

3) Pressurize the chamber and water tank with CO_2 to 6.1MPa and stir the high-pressure water tank for two hours to saturate the water with CO_2. Reduce the temperature of the environmental chamber to 12 °C.
4) Inject CO_2 saturated water into the sediment chamber. Control the pressure gradient.
5) Inject high pressure CO_2 (10MPa) into the sediment chamber, and decrease the temperature to 2 °C. Allow time for hydrate formation.
6) Close valves and transport X-ray transparent high-pressure chamber for X-ray imaging, while maintaining PT conditions within the stability field.

The evolution of pressure and temperature during hydrate formation are shown in figures 4 and 5. PT paths show the effects of dissolution, hydrate formation, and highlight differences in response between the internal thermocouple and the boundary one that more closely tracks the imposed boundary conditions.

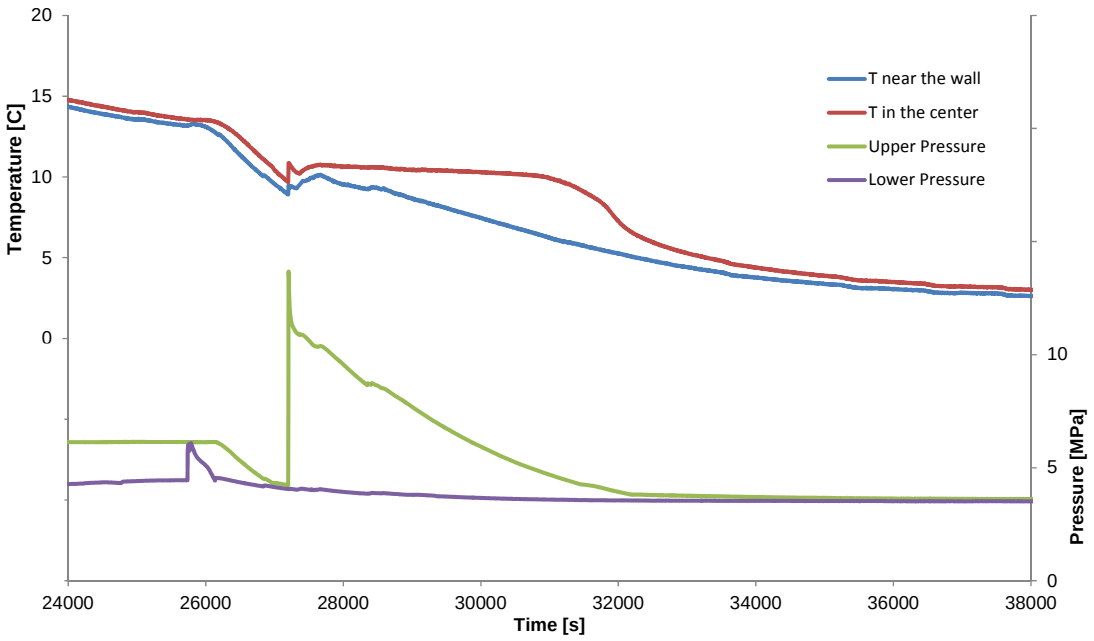

Figure 4. Pressure and temperature signatures. Notation: **T near the wall** is the temperature response of the thermocouple touching the wall, **T in the center** is the thermocouple within the sample, **Upper pressure** is the pressure response recorded by the pressure transducer at the top of the chamber, and **Lower pressure** is the lower pressure transducer. Note: the upper pressure transducer is always on-line; the lower transducer is on line when needed to measure pressure gradients.

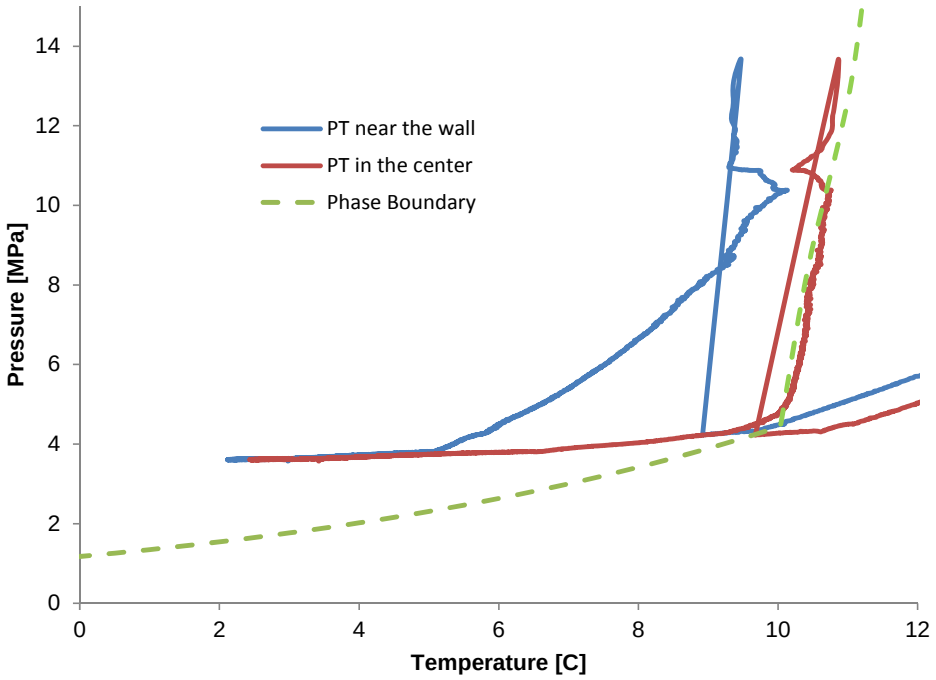

Figure 5. PT trajectory imposed on the diatomaceous sediment. Note: the paths shown begin outside of CO_2 hydrate stability.

After the first CO_2 injection, the X-ray transparent high-pressure sediment chamber was transported to the scanner for X-ray imaging. To minimize warming time, only selected X-ray projections were gathered for this test. Afterwards, the sediment chamber was replaced into the environmental chamber and subjected to a second flooding with CO_2 saturated water. PT signatures are shown figure 6.

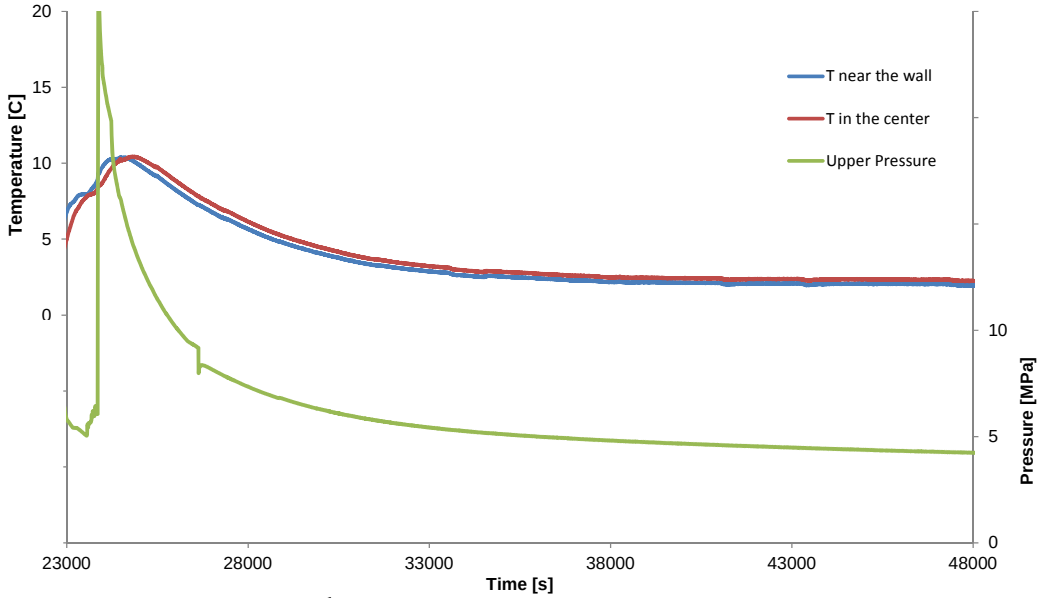

Figure 6. PT signatures during 2nd injection.

Finally, a second set of X-ray projections was gathered (figure 7). The X-ray images show clear structures in the sample. Darker zones correspond to higher mass density. Considering the extreme low density of dry diatoms (as low as 0.33g/cm^3), the darker zone may represent a hydrate lens – this will be corroborated as this experiment continues with additional flooding-imaging cycles and a full tomographic scan.

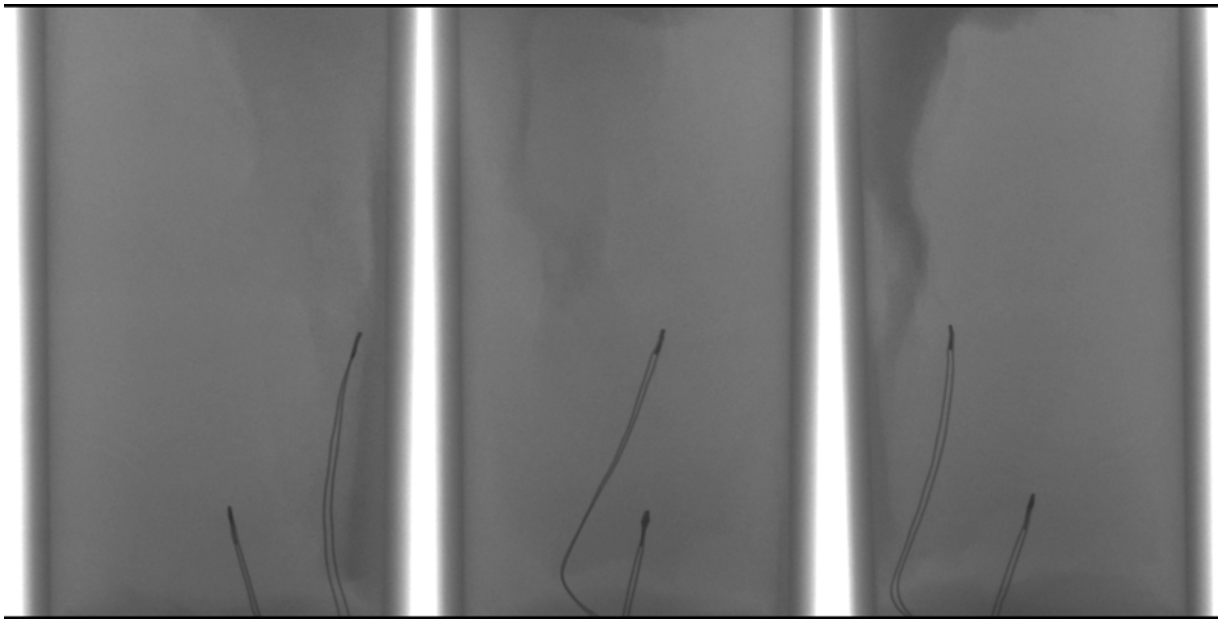

Figure 7. X-ray projections at three rotations after the 2nd injection (the two pairs of wires are the thermocouples).

Thermal Analysis of the X-ray Transparent High-pressure Chamber

The warming rate of the sediment filled aluminum chamber when exposed to standard room temperature conditions limits our ability to conduct high resolution full-tomographic studies. Therefore, the chamber was subjected to varying degrees of insulation to design the X-ray scanning procedure.

Ambient Heating. The change in temperature can be described by Newton's Law of cooling/heating

$$\frac{\partial T}{\partial t} = -\alpha\left[T(t) - T_{amb}\right]$$

$$T(t) = T_{amb} + \left(T_0 - T_{amb}\right)e^{-\alpha t}$$

where: T_{amb} is the ambient temperature, T_0 is the initial temperature, and α is the heating coefficient. The heating coefficient α is proportional to the exposed area of the object and inversely proportional to the specific heat capacity of the materials. Therefore, the temperature of the object will exponentially evolve after a step change in the environment temperature (figure 8).

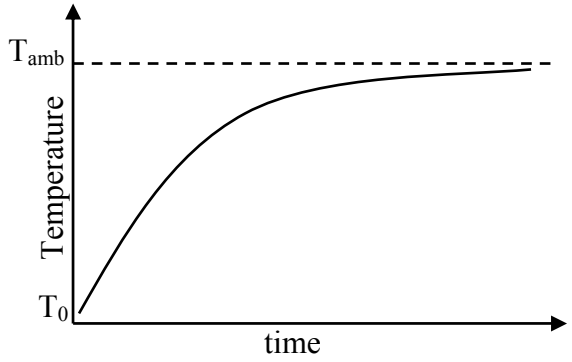

Figure 8. General trend for the heating of an object.

Experiment Design. Kaolinite at a water content of 50% was used to fill the chamber. Then, the chamber was homogeneized at T= 0.5°C. Finally, it was exposed to room temperature while protected using different X-ray invisible insulation systems. Results and fitted trends are shown in Table 1.

Table 1. Results of the aluminum chamber thermal analysis.

Experimental Setup	Temp @ 35 min [°C]	Time @ 9.8°C [min]	α [min^{-1}]
1) No Insulation	11.1	27.7	0.0144
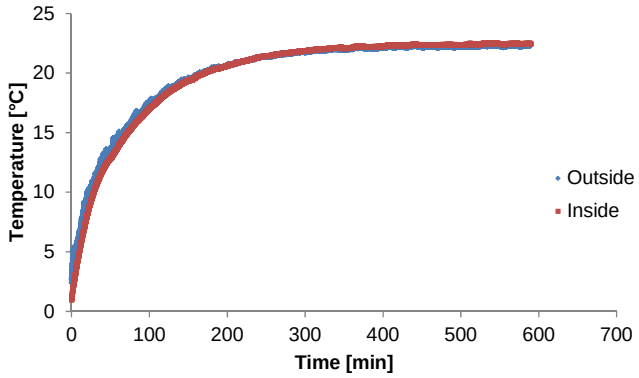		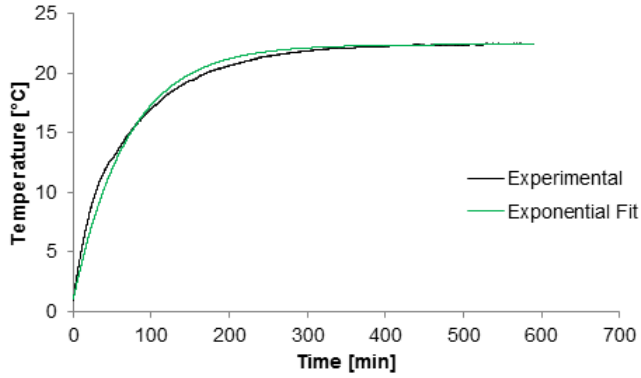	
2) Insulated Box	8.6	45	0.0088
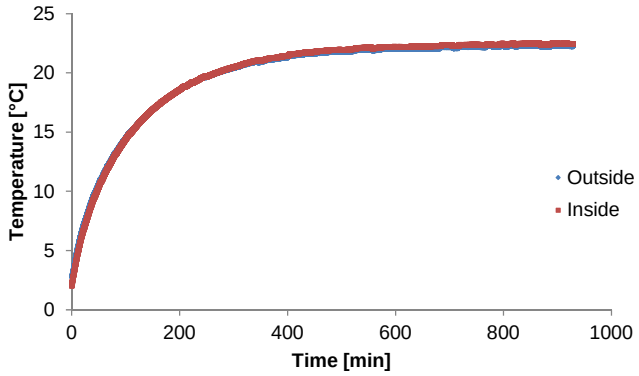		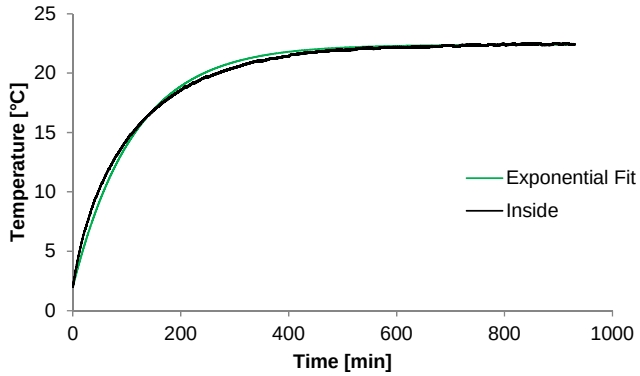	
3) Insulated Box + Wrap	6.5	63	0.0083
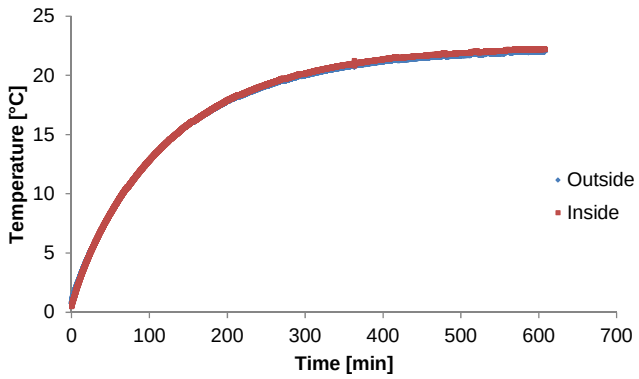		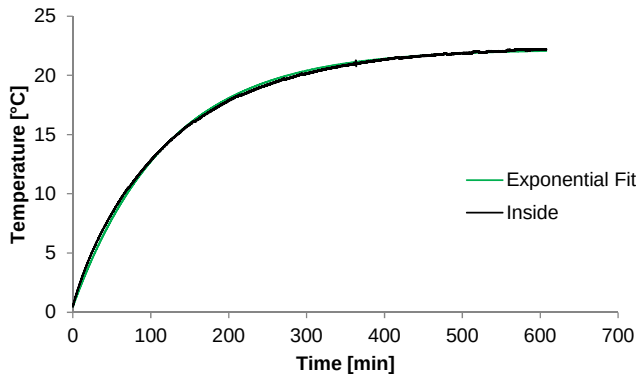	

Numerical simulation. A more detailed study was conducted using numerical simulation in COMSOL on a 3D CAD model of the aluminum chamber filled with a material with similar bulk properties as the clay paste experiment. Global model results agree with experimental data and provide detail information about upper and lower boundary effects.

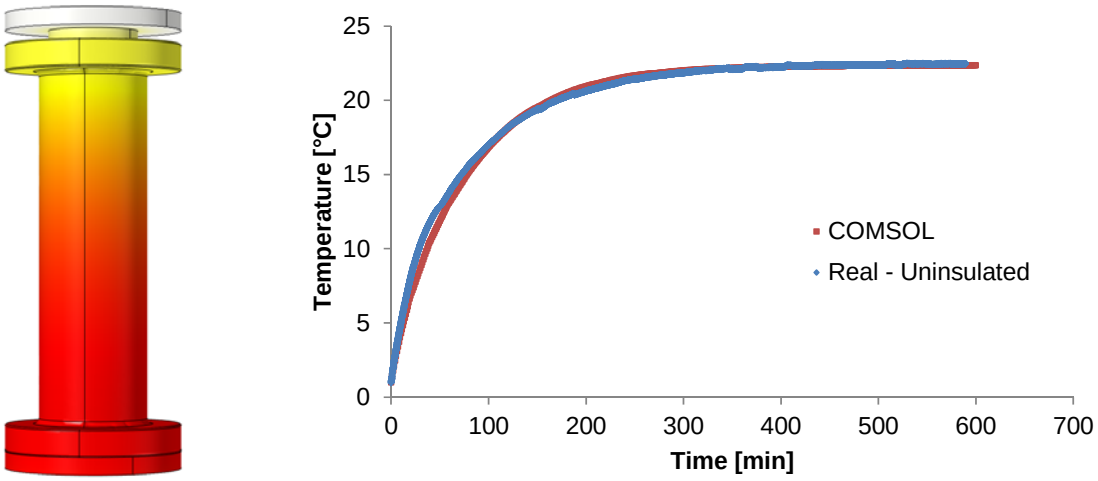

Figure 9. COMSOL model and temperature signature at a point that corresponds to the location of the thermocouple in the experimental test.

A Full 3D model of the aluminum chamber, which is shown in figure 10, was created for numerical modeling and to test compatibility when designing the X-ray Scanner base mount attachment.

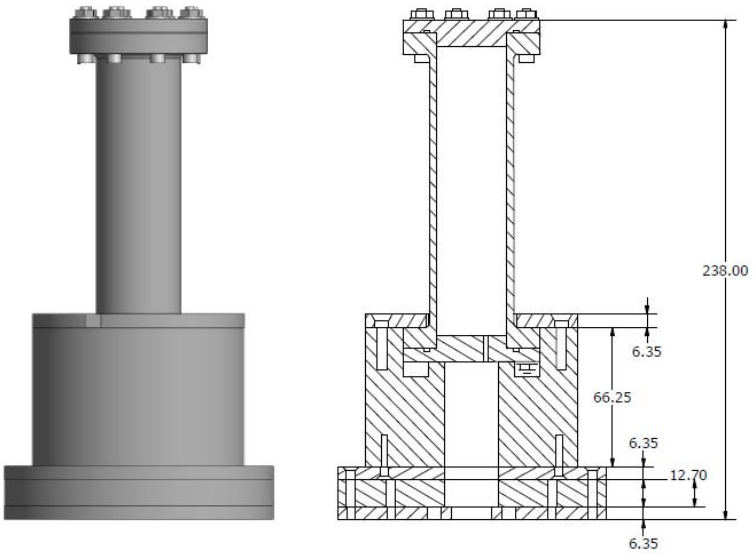

Figure 10. 3D model and cut-section of the aluminum chamber and X-ray motor mounting base.

Small-strain Stiffness - Analytical Study

Pronounced morphological differences between hydrate formation in coarse- and fine-grained sediments, prompt us to use models to anticipate effective medium properties of hydrate-bearing clayey sediments given a continuous matrix material and one or more inclusions at a known volume fraction within the matrix. Solutions such as differential method, generalized self-consistent, and Mori-Tanaka (Christensen 1989) and micro-mechanics models (e.g., solutions developed for fiber composites) are available.

For this study, the results from the self-consistent method for disconnected disks and penny-cracks are compared against the typical effective medium bounds, Series and Parallel and Hashin-Shtrikman Lower and Upper bounds. Model results are plotted in figure 11 (see common elastic property data for fine-grained hydrate system in table 2 – Numerical simulations in progress).

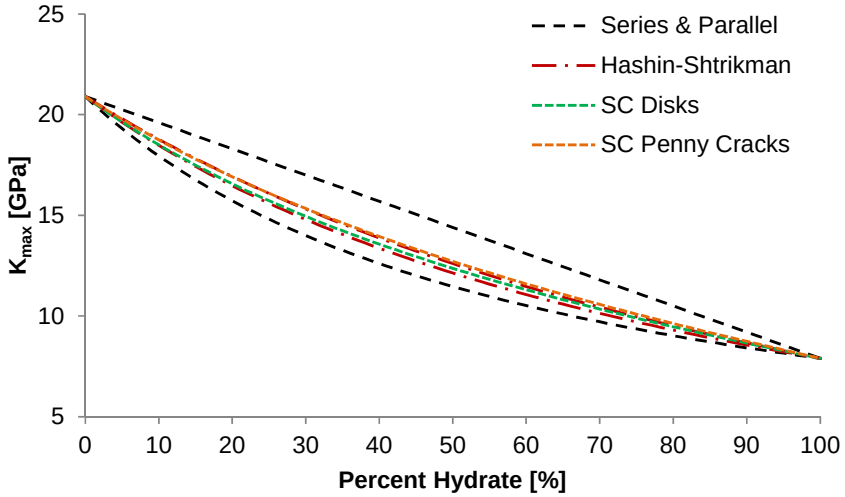

Figure 11. Effective medium model comparison

Table 2. Elastic wave velocities and modulus for hydrate system elements.

Source	**Material**	**V_P [m/s]**	**V_S [m/s]**	**K [GPa]**	***v***
Bathe 1984	THF Hydrate	3513	1663	8.27	0.355
Gold 1958	Ice Ih @ 268 K	3870	2020	8.72-11.3	0.31-0.36
Helgerud et al 2009	Ice Ih	3878	1948	9.2	0.331
	Methane Hydrate sI	3777	1961	8.5	0.315
Waite et al. 2006	Ice Ih @ 260 K	3900	1970	9.0	0.33
	Methane Hydrate, sI	3650	1890	7.1	0.317
Mavko et al. 2009	Clay			20.9	

MILESTONE LOG

Milestone	Planed completion date	Actual completion date	Verification method	Comments
Literature review	5/2013	5/2013	Report	Completed first phase. Will continue throughout the project
Preliminary laboratory proto-col	8/2013	8/2013	Report (with preliminary val-idation data)	this and previous reports
Cells for Micro-CT	8/2013	8/2013	Report (with first images)	this and previous reports
Compilation of CT images: segregated hydrate in clayey sediments	8/2014	In progress	Report (with images)	
Preliminary experimental studies on gas production	12/2014		Report (with images)	
Analytical/numerical study of 2-media physical properties	5/2015	In progress	Report (with analytical and numerical data)	
Experimental studies on gas production	12/2015		Report (with data)	
Early numerical results related to gas production	5/2016	In progress	Report	
Comprehensive results (in-cludes Implications)	9/2016		Comprehensive Report	

PRODUCTS

- **Publications:**

  In progress

- **Presentations:**

  In progress

- **Website:** Publications and key presentations are included in http://pmrl.ce.gatech.edu/ (for academic purposes only)
- **Technologies or techniques:** X-ray tomographer and X-ray transparent pressure vessel
- **Inventions, patent applications, and/or licenses:** None at this point.
- **Other products:** None at this point.

PARTICIPANTS & OTHER COLLABORATING ORGANIZATIONS

Research Team: The current team is shown next. We anticipate including external collaborators as the project advances

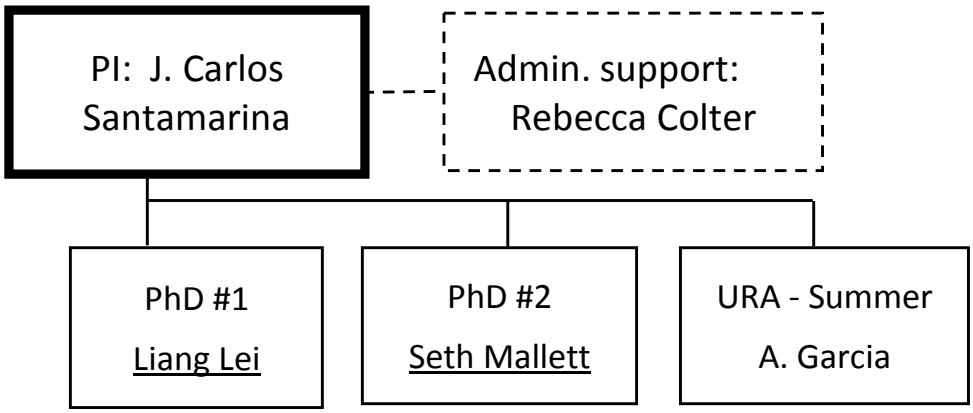

IMPACT

While it is still too early to assess impact, we can already highlight preliminary success of exploring hydrate lenses morphology in real systems, and analogue studies using a high resolution tomographer.

CHANGES/PROBLEMS:

None at this point.

SPECIAL REPORTING REQUIREMENTS:

We are progressing towards all goals for this project.

BUDGETARY INFORMATION:

As of the end of this research period, expenditures are summarized in the following table.

Note: in our academic cycle, higher expenditures typically take place during the summer quarter.

Baseline Reporting Quarter	Budget Period 1								Budget Period 2				
	Q1		Q2		Q3		Q4		Q1		Q2		
	10/1/12 - 12/31/12		1/1/13 - 3/31/13		4/1/13 - 6/30/13		7/1/13 - 9/30/13		10/1/13 - 12/31/13		1/1/14 - 3/31/14		4/1/1
	Q1	Cumulative Total	Q2	Cumulative Total	Q3	Cumulative Total	Q4	Cumulative Total	Q1	Cumulative Total	Q2	Cumulative Total	Q3
Baseline Cost Plan													
Federal Share	39,212	39,212	39,212	78,424	39,212	117,636	39,212	156,848	39,212	196,060	39,212	235,272	39,2
Non-Federal Share	11,423	11,423	11,423	22,847	11,423	34,270	11,423	45,694	11,423	57,117	11,423	68,540	11,4
Total Planned	50,635	50,635	50,635	101,271	50,635	151,906	50,635	202,542	50,635	253,177	50,635	303,813	50,6
Actual Incurred Cost													
Federal Share	0	0	16,173	16,173	20,191	36,364	66,556	102,920	35,434	138,355	28,305	166,660	
Non-Federal Share	0	0	11,423	11,423	11,423	22,847	11,423	34,270	11,423	45,694	11,423	57,117	
Total Incurred Costs			27,597	27,597	31,614	59,211	77,979	137,191	46,857	184,048	39,729	223,777	
Variance													
Federal Share	-39,212	-39,212	-23,039	-62,251	-19,021	-81,272	27,344	-53,928	-3,778	-57,706	-10,907	-68,612	
Non-Federal Share	-11,423	-11,423	0	-11,423	0	-11,423	0	-11,423	0	-11,423	0	-11,423	
Total Variance	-50,635	-50,635	-23,039	-73,674	-19,021	-92,695	27,344	-65,351	-3,778	-69,129	-10,907	-80,036	

National Energy Technology Laboratory

626 Cochrans Mill Road
P.O. Box 10940
Pittsburgh, PA 15236-0940

3610 Collins Ferry Road
P.O. Box 880
Morgantown, WV 26507-0880

13131 Dairy Ashford Road, Suite 225
Sugar Land, TX 77478

1450 Queen Avenue SW
Albany, OR 97321-2198

Arctic Energy Office
420 L Street, Suite 305
Anchorage, AK 99501

Visit the NETL website at:
www.netl.doe.gov

Customer Service Line:
1-800-553-7681